Pergamon

Bioorganic & Medicinal Chemistry, Vol. 5, No. 6, pp 1021–1035, 1997

PII: S0968-0896(97)00053-9
0968-0896/97 $17.00 + 0.00

Context Dependent RNA–RNA Recognition in a Three-Dimensional Model of the 16S rRNA Core

Benoît Masquida, Brice Felden† and Eric Westhof*,‡

Institut de Biologie Moléculaire et Cellulaire du CNRS-UPR 9002, 15 rue René Descartes, F-67084 Strasbourg Cedex, France

Abstract—A 3-D model of the core of the 16S rRNA of *Escherichia coli* containing 328 residues has been built in the protein map derived from neutron scattering data with the help of all the available phylogenetic, biochemical, and cross-linking data. The three pseudoknots of the 16S-core cluster, through the arrangement of complex three-, four- and five-way junctions, around the neck and at the subunit interface. The roles in assembly, initiation or elongation of the three pseudoknots in ribosomal dynamics are emphasized. The 530-loop, localized on the periphery of the 30S particle, could be built with and without a pseudoknot independently of the state of the particle. The pseudoknot of the central domain controls the dynamics of an helix connected to the subunit interface which could trigger some mechanism during translation. The process of the model construction is compatible with a folding scenario in which the 5′-terminal pseudoknot controls the assembly of the central junction and the subsequent folding of the 3′-major domain. The modelling, together with the phylogenetic analysis and the experimental data, point to several potential RNA–RNA contacts which depend on the structural and sequence context in which they occur. © 1997 Elsevier Science Ltd.

Introduction

The prokaryotic ribosome consists in the association of two nucleoproteic particles sedimenting respectively at 50S and 30S. Two RNAs (23S, 5S) and 34 proteins (L1–L34) interact to compose the 50S subunit, whereas the 30S subunit is composed of the association of only one RNA (16S) and 21 proteins (S1–S21).

From a structural point of view, the 16S rRNA can be subdivided in four domains: the 5′, central, 3′-major, and the 3′ minor domain, each weaving an interaction network with proteins leading to RNP assembly.[1–3] These domains should then interact together cooperatively, as directed by the RNA which constitutes the subunit scaffolding. The 16S rRNA is able to form, in aqueous solution, active 30S subunits by interactions with the 21 small-subunit proteins under conditions controlled by the Mg^{2+} concentration.[3] This self-assembly phenomenon has been shown to be sequential and cooperative.[1–4] These studies show that the primary proteins (S4, S7, S8, S15 and S17) interact first with each 16S domain. This is followed by the binding of the secondary and tertiary proteins, which need previously docked proteins to properly interact with the self-forming subunit. From a hierarchical point of view of RNA folding it seems reasonable to make the assumption that the primary proteins enable the partial folding of some regions in each 16S domain which, linked together by the 16S-core would then interact cooperatively, helped by the secondary and tertiary proteins. This is supported by results from chemical probing experiments.[4–6] Moreover the three 16S pseudoknots (Pk1, Pk2 and Pk3), established by comparative sequence analysis,[7–9] were each demonstrated by mutational analysis to be necessary for translation to occur.[10–12] Pseudoknots are frequently observed in structured RNAs.[13] It has been suggested that they could play a role in RNA folding because they impose stringent constraints on the folding pathway, thereby guaranteeing the absence of misfoldings.[14] It appeared, therefore, interesting to us to assemble a 16S-core containing the three established pseudoknots.

The neutron diffraction-derived 3-D map of ribosomal proteins obtained by Capel and coworkers[15,16] is the only direct physical result concerning the distribution of ribosomal components within the 30S particle. Based on such a map and additional biochemical data, three ribbon structure models have been published.[5,17,18] They aim to incorporate simultaneously the major part of the available biochemical data such as probing or footprint information[6,19–22] and the RNA–RNA and RNA–protein crosslinking experiments (reviewed in the literature[23]). These models, in which the RNA structure is approximated with cylinders or ribbons linking the phosphorus atoms, partially describe the path of the 16S RNA through the 30S subunit by fitting of the biochemical constraints into the neutron map.

In this work, considering the underlying importance of some 2-D elements both in the structuring of the native particle and in function during translation, we have defined a 16S-core (Fig. 1). We then built a full atom 3-D model of this 16S-core which enables us to focus on

†Present address: Howard Hughes Medical Institute, 6160 Eccles Genetics Building, University of Utah, Salt Lake City, UT 84112, U.S.A.
‡Phone: 33-88-417046; Fax: 33-88-602218; e-mail: westhof@ibmc.ustrasbg.fr

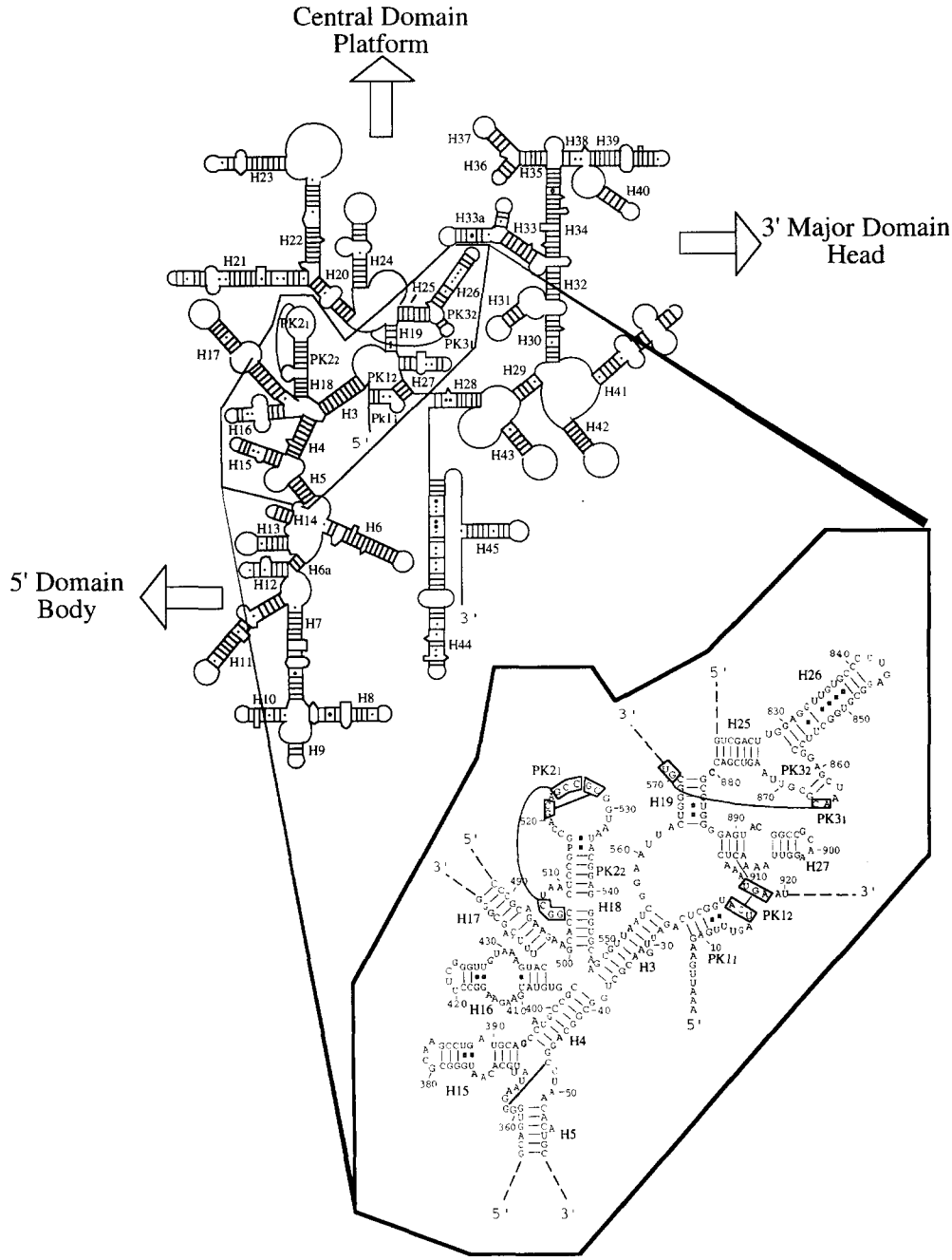

Figure 1. A wire-frame secondary structure of the 16S rRNA molecule showing the modelled core of the molecule delineated with a polygon and enlarged. The focus on this region indicates the base-sequence (1–58/354–446/488–571/821–920) and the phylogenetically proven interactions comprising the three pseudoknots. The drawing is adapted from Gutell et al.[42] with slight changes as discussed in text.

the relative localization of the pseudoknots and to presume on their role during self-assembly and translation.

Results

The base numbering is according to *E. coli* 16S ribosomal RNA. The topology of the model is described within the scaffold of the ribosomal protein map, viewed from the interface side (Fig. 2) in a three orthogonal axis system (x, y, z) (x: 30S left side to plateform; y: 30S bottom to top; z: solvent side to interface side).

Definition of the 16S-core RNA

When looking at the 30S particle from the 50S interface, the RNA domains are organized as follows. The 5′-domain is subdivided in two sub-domains ($5'_1$, $5'_2$), where $5'_1$ encompasses the first pseudoknot (Pk1)

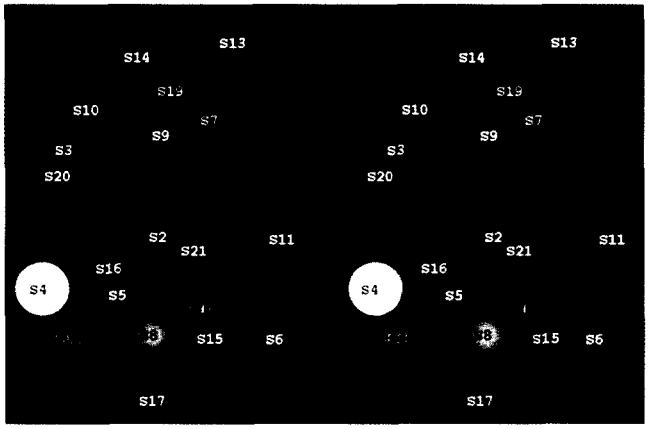

Figure 2. Stereo pair of the ribosomal protein map derived from neutron-scattering.[15,16] The view is from the 50S interface side and proteins S2–S21 are represented. The radii of gyration have been reduced by 5 Å for clarity. Apart from S7, which was used as a distance constraint towards the 3′-end of the model of the 16S core, all the coloured proteins (S4, S5, S8, S12 and S18) are in direct contact with the model.

and its junctions to the contiguous helices. The $5'_1$-domain can be considered as the linker between the other domains. It takes place inside the subunit neck in the neighbourhood of S2 and S5, as indicated by the distance between the central pseudoknot (Pk1) and the binding site of ribosomal protein S7 (Table 1). The second subdomain, $5'_2$, contains the helices ranging from H3 to H18 and the second pseudoknot, Pk2. It is footprinted by proteins lying on the left side of the subunit from middle-body to the neck, S4, S12, S16, S17 and S20. The central domain, encompassing helices H19–H27, interferes with proteins located in the platform, S8, S11, S15, S6/S18, S21. The major 3′-domain emerges from Pk1, coils up S7 and finally interacts with all the head proteins. The minor 3′-domain is more difficult to localize with accuracy as it is linked to the core of the molecule by a flexible seven nucleotide-long junction that increases the number of relative positioning of this domain towards the others. Nonetheless the 3′-domain is footprinted by S20, which is able to form a stable complex with the RNA, and by S16,[6] which intervenes on a later stage of 30S subunit self-assembly. But strong biological evidence, such as the A (Aminoacyl–tRNA) and P-site (Peptidyl–tRNA) localization in the 1400–1500 region or the presence of the Shine-Dalgarno sequence, converges to the view that this domain lies in the 30S cleft at the subunit interface. In summary, the 16S-core consists of $5'_1$ ($Pk1_1$, $Pk1_2$), the starting helices of both $5'_2$ (H3, H4, H5, H15, H16, H17, H18, $Pk2_1$, $Pk2_2$) and the central domain (H19, H25, H26, $Pk3_1$, $Pk3_2$, H27) ending with residue U920 (Fig. 1).

Modelling strategy applied to the 16S-core RNA

The relationships between some RNA regions and the ribosomal proteins were taken into account for docking the 16S-core into the 3-D protein map obtained by neutron diffraction methods[15,16] while simultaneously incorporating the major part of biochemical data. Despite the high quality of the footprint and crosslink results, the widely separated experimental conditions endanger the modelling approach. Crosslink experiments are usually performed on the 30S particles and footprints are realized on self-assembling subunits, implying important differences between the conformational states of the 16S in both experiments. Thus, we defined an initial set of constraints, based on biochemical data, following several criteria which guarantee the convergence of independent experiments. For footprint and crosslink experiments, an RNA region was assigned close to a given protein only when the crosslinked residues were overlapping the footprinted ones. The incorporated intra-RNA crosslinks should be observed in vivo prior to in vitro or both, since this gives confidence concerning the native state of the subunits.[24] Next we took into account the length of the RNA helices to pin some nucleotides towards a protein centre of mass. Focusing on different sections of the 16S-core RNA, it was possible to exhibit three regions, fulfilling the defined criteria. We defined these regions as anchor points for the modelling (Table 1), since different types of experiments were yielding converging results. The resulting constraints added to those due to torsional angles provide powerful means to reduce the number of degrees of freedom of the model.

The first anchor point (Table 1) involves mainly S4 through three different kinds of experiments which strongly converge to a location of S4 near H16. The close vicinity of S4 to S12 is well correlated with the two protein footprints on H18/PK2. Furthermore, both Pk2 and S12-mutants have been shown to express a streptomycin resistance (SmR) phenotype, respectively.[25–29] Otherwise, the tRNA-dependent protection of G530 from kethoxal, increased in hyperaccurate ribosomes, stemmed from a streptomycin-dependent S12-mutant strain.[30] The outcoming connection between S12 and Pk2 is reinforced by base-probing studies which led to the conclusion that the pseudoknot structure was stabilized by this protein[5] and immuno-electron microscopy which located both S12 and the 530-loop in the same region of the 30S subunit.[31,32] Intra-RNA crosslinks are useful to assess the relative location of several helices. The most important crosslink involves residues 31 and 48[24,33] and led to the placement of H4 perpendicularly to H3. The second anchor point implicates the site of interaction of S7 on the RNA and compels U920 to belong to an area located between S4 and S7 within a distance greater than 50 Å from the centre of mass of S7 due to the length of H28 and to the first anchor point. The third anchor point places the 840-loop in the vicinity of S18.

With this set defined, the next step consisted of applying stereochemical constraints in the RNA model. The following modelling rules were applied. Experimental errors in the coordinates of the neutron map[16] together with the ellipsoidal shape of ribosomal proteins[34–36] enable slight interpenetration of the RNA model within

Table 1. Summary of the constraints used in the modelling. The first column describes the nature of the constraint used. The regions where the constraints take place are located in the second and third columns. The consequences of the experimental data are given in the fourth column with the references

Experimental constraint	Involving	Area of effect	Consequences (reference)
Intra-RNA constraints			
UV-crosslink	**G31/C48**	H3 and H4	This short-length crosslink forces H3 to be perpendicular to H4.[33]
UV-crosslink	**A366-G369/ A397-G399**	H4 and H15	The junction 360–366 is placed in the shallow groove of H4 with stacking between crosslinked residues.[24]
First anchor point			
FeII EDTA footprint	**S4**	H16 (405–412, 427) H17 (437–440) H18 (500–504, 541–543)	In the initial constraint set, only the strong FeII EDTA protections have been considered.[6]
FeII EDTA probing	**S4** (Cys 31)-FeII	H16 (419–432)	The targeting of residues from H16 by hydroxyl radicals generated in the vicinity of S4 confirms the localization of this protein near H16.[50]
Nitrogen mustard crosslink	**S4**	H16 (413)	The fact that crosslinked and footprinted sites on the 16S are overlapping constitute additional strong evidence for the localization of S4 near H16.[70]
Mutational analysis	**S12**	530 loop	The tRNA-dependent protection of G530 is antagonized in a streptomycin-dependent (SmD) S12-mutant strain. Otherwise, independent mutations both in Pk2 and S12 lead to streptomycin resistance (SmR).[25–30]
Electron microscopy	**S12** 530-loop	The neck of the 30S particle at the interface side of the subunits	Both S12 and the 530-loop have been located in the same region of the 30S subunit, respectively, by immuno electron microscopy and DNA-hybridization electron microscopy.[71,72]
Base-probe footprint	**S12**	$Pk2_1$ (505–506) $Pk2_2$ (535) 530-loop (520–524)	The folding of the 530-loop depends on S4 and S12.[5]
FeII EDTA footprint	**S12**	$Pk2_2$ (515–517, 534–538) 530-loop (518–524)	FeII EDTA probing experiments show the specific protections of nucleotides involved in Pk2 folding. At the end of the modelling, the conformation of the 5-way junction was consistent with S12-dependent protections on H3.[6]
Second anchor point			
APAI[54] and imminothiolane[73] crosslink	**S7**	H30 (1238–1240)[54] H43 (1377–1378)[73]	As in the case of S4, crosslinked nucleotides are overlapping the footprinted ones. Such a convergence is a good argument to involve this region in S7 site formation.[54,73]
FeII EDTA footprint	**S7**	H29 (935–950, 1340–1346) H30 (946–950, 1230–1239) H41 (1250–1255, 1287–1292) H42 (1307– 1312, 1320-1323, 1328–1329) H43 (1348–1384)	This cluster of helices is, according to footprinting and crosslinking studies, well localized around S7. So we assume that residues 934 and 1384 should be in the neighbourhood of S7. The length of H28 (12 base-pairs ⇒34.8 Å) forces U920 to be separated from S7-site by a distance greater than 40 Å.[6]
Third anchor point			
FeII EDTA footprint	**S6/S18**	H22 (670–672, 735–738, 742) H23 (673–676, 714–719) H26 (829–836, 843, 850)	The central domain is protected from chemical attack only by proteins constituting the platform of the 30S particle as S6 and S18. The dimer S6/S18 is able to bind the 16S which could generate long-distance protections overlapping the S15 site.[6]
Nitrogen mustard crosslink	**S18**	H26 (845–851)	This crosslink belongs to the category of crosslinks that overlap the footprinted site as are those concerning S4 and S7.[70]

the spheres representing the proteins. The RNA secondary structure was extensively checked using the Ribosomal Database Project (RDP) facility.[37] Sequence analysis emphasized the conservation of junction lengths among the prokaryotic ribosomes and pointed to the conservation of some nucleotides (Table 2).

Table 2. Phylogenetic analysis of the junctions in the core of the 16S rRNA, based on 2844 sequences from *Prokaria* available at the Ribosomal Database Project (RDP[37]). The number of valid sequences corresponds to the subset of sequences for which the checked positions have been correctly sequenced and aligned. The frequencies correspond to the ratio of the number of sequences presenting a typical pattern for given positions over the number of valid sequences

Junction	Junction length (residue numbers)	Sequences (90% ≤ Σ ≤ 100%)	Frequencies % (*Bacteria*)	Frequencies % (*Archaea*)	Number of valid sequences (%)
H1/H3	1 (26)	**A**	**100**	**95**	1731 (61)
H3/H4	1 (38)	G[a]	**90**	—	2130 (75)
		A	7	**98**	
H4/H5	4 (47–51)	CC**UA**A[a]	**45**	—	2223 (78)
		C**UUA**A	39	—	
		U**CUUA**	3	—	
		C**UUUA**	3	—	
		G**CUA**A	—	**51**	
		G**UUA**A	—	27	
		G**UUUA**	—	11	
H5/H15	7 (360–366)	AA**GAA**UC	2	—	2521 (89)
		AG**GAA**UA	5	—	
		AG**GAA**UC	2	—	
		GC**GAA**AA	—	30	
		GC**GAA**AC	—	**52**	
		GG**GAA**UA[a]	**50**	—	
		GG**GAA**UC	18	—	
		GG**GAA**UU	13	—	
H15/H4	1 (394)	**G**	**99**	**100**	2545 (89)
H4/H16	2 (404–405)	**GU**	**96**	**97**	2512 (88)
H17/H18	2 (498–499)	**AA**	**96**	**97**	2460 (87)
H18/H3	1 (546)	A[a]	**39**	35	2437 (85)
		G	26	**63**	
		N	19	—	
		U	14	2	
H3/H19	7 (557–563)	**GCUUUA**	—	**16**	2459 (86)
		GGAAUCA	13	—	
		GGAAUUA[a]	**54**	—	
		GGAUUCA	1	—	
		GGAUUUA	20	—	
		GGGAUUA	1	—	
		GUGAUUA	—	10	
H25/H26	1 (828)	A	**77**	**69**	2502 (88)
		C	4	10	
		U[a]	12	20	
H29/$Pk3_2$	3 (858–860)	AC**A**	3	—	2485 (87)
		GA**A**	13	**42**	
		GC**A**	**39**	—	
		GG**A**[a]	10	—	
		GU**A**	20	25	
$Pk3_2$/H25	4 (859–862)	AAU**A**	7	—	2484 (87)
		AUUA	**44**	—	
		GAU**A**	12	—	
		GUG**A**[a]	6	36	
		GUU**A**	22	**46**	
H25/H19	1 (880)	**C**	**94**	**96**	2467 (87)
H19/H27	1 (887)	**G**	**100**	**99**	2476 (87)
H27/Pk1	3 (912–915)	**AAA**	**98**	**99**	2324 (82)

[a]Sequences corresponding to *E. coli*.

Finally, the stacking possibilities for adjacent helices were chosen according to observations from the crystal structures of the tRNA and the hammerhead ribozyme.[14,38,39]

Modelling of the three pseudoknots

Pk1. Pk1 (Fig. 3) belongs to the classical type (ii) pseudoknot according to the nomenclature of Westhof and Jaeger.[13] The first stem 9–13/21–25 ($Pk1_1$) is able to stack on the second one ($Pk1_2$), which involves base-pairings between residues 17–19 from the 14–19 loop and nucleotides 916–918 from the end of the central domain. Since a U-turn with a C or G occurs in seryl-tRNA from the Candida group,[40] an anticodon-like shape was given to the seven-nucleotide loop 14–19. Since U20 is not reactive to kethoxal both in naked-16S and in 30S subunit,[41] it is stacked between the two pseudoknotting stems to interact with U14 (Table 3) as

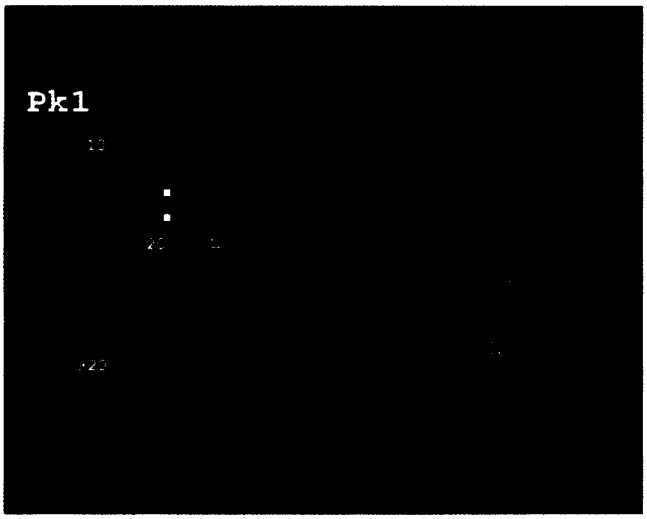

Figure 3. The figure shows the secondary structure of the 16S RNA central pseudoknot, Pk1 (left part). This type (ii) pseudoknot is formed by the interaction of the 14–20 loop (green) with the 3′-end of the central domain (purple). The ribbon model (right part) shows the stacking of stem $Pk1_1$ (red) and stem $Pk1_2$ (green and purple) with the proposed non-canonical base-pairs U13/G21 and U14/U20 (but comparative sequence analysis does not yield covariations) A915 (blue) exits from H27 and possibly interacts with U20 (see Table 3).

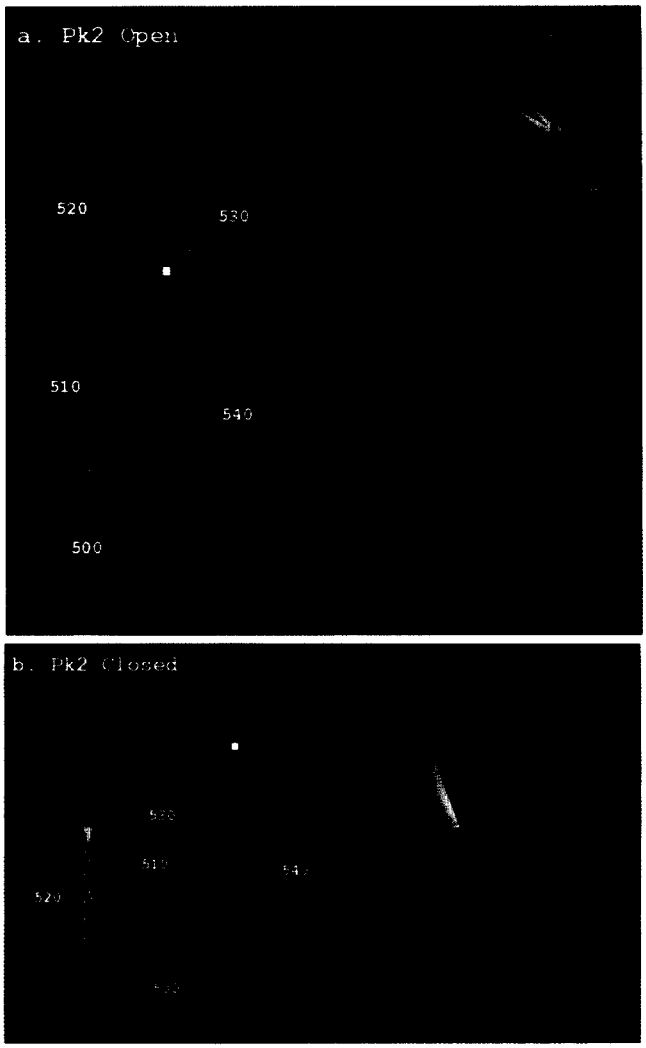

Figure 4. Several biochemical studies have led to the conclusion that the 530 loop could adopt an open (a) and a closed (b) conformation.[30] In the open model, $Pk1_2$ (blue) stacks on H18 (red) and is extended by additional base-pairs in the apical loop (orange), while the six nucleotide bulge (green) interacts with residues from the shallow groove of H18 (Table 3). The conformational change from the open to the closed form progresses through the collapse of the orange stem along $Pk2_2$ to allow residues 524–526 to base-pair with residues 505–507 thereby forming the pseudoknot. It is worth noting that G530 (purple sphere), protected from kethoxal attack when the A-site tRNA is bound to the ribosome,[69] is base-paired with C518 in the open form, while widely accessible at N1 in the closed form.

is the case in anticodon loop for residues 32 and 38. Moreover, to maximize stacking interactions between $Pk1_1$ and $Pk1_2$, A915 is set in the shallow groove of Pk11 and interacts with U20.

Pk2. Pk2 (Fig. 4) corresponds to a subclass of type (ii) pseudoknot with a loop (L2) between the 5′ strand of S2 and the 3′ strand of S1. Residues 505–507 from the 505–510 bulge interact with nucleotides 524–526 in the apical 530-loop to form the first stem ($Pk2_1$) of the pseudoknot structure, while the canonical helix 511–517/534–540 forms the second stem ($Pk2_2$). With $Pk2_2$ in continuity with H18, stereochemical constraints plead for coaxial stacking of $Pk2_2$ and H18 in a right-handed manner. Thus, $Pk2_1$ has to flank the coaxial stems while avoiding a crossing-over of the junctions 518–523 and 527–533. This topology forces $Pk2_1$ to adopt a colinear orientation with the coaxial helical stems H18/$Pk2_2$ and pushes the bulge against H18. As a consequence, A509 and A510 are able to interact in the shallow groove of H18 with base-pairs C503/G542 and C504/G541 (Table 3), respectively. Although tertiary interactions involving Watson–Crick interactions between G521/C528 and C522/G527 were phylogenetically suggested,[42] they were not introduced into the described model as it is very unlikely to form base-pairs within the connecting strands of the closed pseudoknot. Since a dynamic role for Pk2 has been proposed,[30,43] we built another model in which the pseudoknotting base-pairs are dissociated and nucleotides within the 530-loop proposed to be involved in tertiary interactions[42] are base-paired. Simultaneously, pairs C518/G530 and C519/G529 are formed to extend the stem as they are likely in 98% of the sequence set. This model leads to an extended H18/$Pk2_2$ hairpin in which the 6-residue bulge stands in the shallow groove of H18, an identical feature to the closed model, which enforces the stacking interactions at the junction between H18 and $Pk2_2$. Therefore the coexistence of both the open and closed forms could explain the different phylogenetic tertiary interactions involving pseudoknotting and base-pairing within the 530-loop. The dynamics of the pseudoknot closing is easy to imagine with these models. Starting from the open structure, a slight left-handed rotation of the closed 530-loop would break the base-pairs from the top of the hairpin (C518/G530, C519/G529, G521/C528, C522/G527), leading to a collapse along $Pk2_2$ and to the closing of $Pk2_1$, a process helped by S12.[30,44] We could conclude from these models that Pk2 dynamics are

Table 3. Proposed tertiary contacts in the core of the 16S rRNA as suggested by modelling studies and supported by phylogenetic analysis of 2844 sequences from *Prokaria* available at the Ribosomal Database Project (RDP[37]). See Table 2 for general explanations

Tertiary contacts	Frequencies	Number of valid sequences (%)
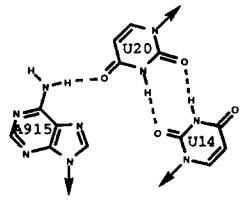	**U14·U20·A915 (95%)**	**1527** (57)
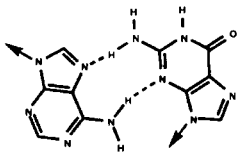 Sheared G·A	**A51·G360 (88%)** A51·A360 (12%)	**2172** (76)
	A860·G869 (43%) A860-A866 (50%)	**2458** (86)
	G362·A366 (59%) G362-C366 (26%) G362-U366 (15%)	**2463** (87)
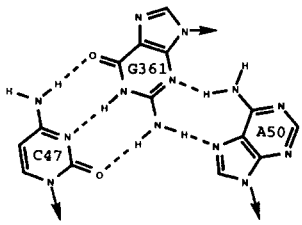	**C47-G361·A50 (85%)** C47-G361·U50 (5%) G47-C361·A50 (4%) U47-A361·U50 (3%)	**2151** (76)
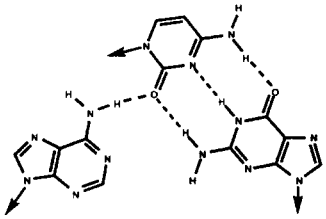	**C503-G542·A509 (71%)** A503-U542·A509 (21%) U503-A542·A509 (6%)	**2255** (79)
	C504-G542·A510 (93%)	**2279** (80)
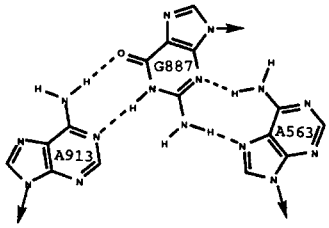	**G88** **7-A913·A563 (100%)**	**2220** (78)
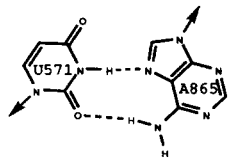 Hoogsteen *trans*	**U571-A865 (100%)**	**2357** (83)

structurally independent of the 16S-core, assuming no structural changes in other regions of the molecule.

Pk3. Pk3 (Fig. 5) is structurally the most complex pseudoknot of the 16S RNA. This type (iii) pseudoknot involves base-pairing between G570–U571/A865–C866 ($Pk3_1$) and G861–C862/G867–C868 ($Pk3_2$). The sequence of the 863–866 tetraloop is 79% of the time UAAC and varies to GAAA in 7% of the sequence set. A GNRA-like conformation for that loop would imply that U571 interacts with A865 in an Hoogsteen-*trans* fashion rather than Watson–Crick, while $Pk3_2$ adopts a

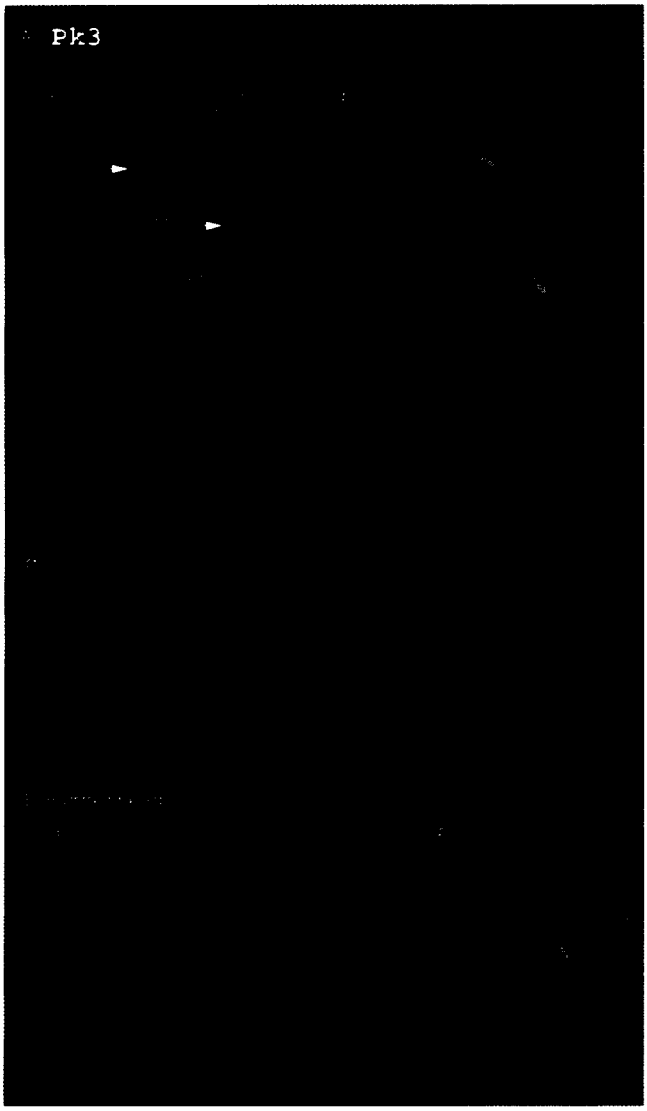

Figure 5. The likely structural analogy between the pseudoknot of the central domain of the 16S, Pk3 (A) and the hammerhead ribozyme (B) is illustrated. Secondary structures are given (a), as well as ribbon models (b), in an orientation showing that they are almost superimposable (see text). A stereo pair of the motif of interaction leading to $Pk3_1$ closure is represented in (c). G570 (red) forms a Watson–Crick pair with C866 (orange), the N4 atom of which interacts with U863 (orange) O2 to form a hydrogen bond. The Hoogsteen interaction of U571 (red) with A865 (orange) is also clearly seen.

standard RNA helix conformation. The conformation of the loop could constitute the beginning of an explanation for the universal conservation of the pair U571–A865. $Pk3_1$ and $Pk3_2$ stack coaxially easily but they belong to the cluster of helices H19/H25/H26 connected to each other with three or less nucleotides. In fact, it seems improbable that stems from Pk3 stack with any of the other helices for at least two reasons. First, the short junctions between any of the adjacent helices do not give sufficient leeway for the intercalation of Pk3 with optimized stacking interactions. Second, the purine-rich pattern of the junctions 858–860 and 869–872 is sufficiently conserved across the phylogeny (Table 2) for trying to find a motif built-up from three helices, one linked to the others with purine-rich junctions. Both arms of the resulting Y-shape structure should, in addition be close enough, in a quasi-colinear way, to allow their linkage through the pseudoknot closure.

The hammerhead ribozyme presents this type of pattern, its stem II is fixed on stem I and III by an asymmetrical purine-rich junction which confers flexibility to the hinge region while conserving the strength of stacking interactions. We, thus, tried to superimpose our model on the available crystallographic structure models,[38,39] assigning the different stems as follows: stem I to H25, stem II to Pk3 and stem III to H26.[14] This approach led to a structure model of Pk3 in which the backbones follow a similar topology, with a junction from Pk3 to H25 containing a U-turn. Nonetheless the junctions, which are shorter than in the hammerhead, force shallow grooves of Pk3 and H25 to face each other instead of their deep grooves as is the case in the hammerhead. Some common features are still maintained: H25 is slightly left-handed towards H26 resulting in the loss of the coaxial orientation while stacking interactions between Pk3 and H26 are optimized through the 4-nucleotide long purine-rich junctions. On the other hand, the presence of a 'sheared' A·G pair, first observed in DNA,[45] involving A860 (N7, N6) and G869 (N2, N3) and corresponding to base-pair A9–G12 in the hammerhead,[38] forces strongly Pk3 to be in a right-handed orientation towards H26. The A·G mismatch (45% of cases) was shown to covary to an A·A mismatch in 50% of cases. In the A·A base-pair, the $AN_7\cdots H_2{-}N_2G$ hydrogen bond could be replaced by a $AN_7\cdots H_2{-}C_2A$ H-bond, since C-H groups adjacent to nitrogen atoms are able to form short C–H···O, C–H···N or C–H···Cl hydrogen bonds.[46] Similar A·G/A·A covariations have been observed by comparative sequence analysis in other systems.[47] Such a contact has also been recently seen in a RNA crystal structure.[48] H19 is then attached to the hammerhead-like model. Its 3′-strand is linked to H25 in a right-handed manner directing the 5′-strand towards the shallow groove of Pk3 and a sharp turn at C569 enables the junctions with $Pk3_1$. H19 constrains the three-way junction (H25, H26 and Pk3) which would become loose while the pseudoknot opens. This raises the possibility that H19/H25/H26/Pk3 exists in a 'tight' and a 'loose' form, which may play some role during translation.

The five-way junction

The five-way junction (5WJ) takes place in a region mainly occupied by ribosomal proteins S4, S5 and S12 and encompasses helices H3, H4, H16, H17, H18 and Pk2 (Fig. 6). As concluded from the Pk2 models, we assume that the global conformation of 5WJ does not depend on the opened and closed states of Pk2. 5WJ modelling is based on the biochemical constraints defined in Table 1 as the first anchor point.

The model of the closed form of Pk2 (Fig. 3b) is readily positioned in the 3-D protein map (Fig. 2), as both

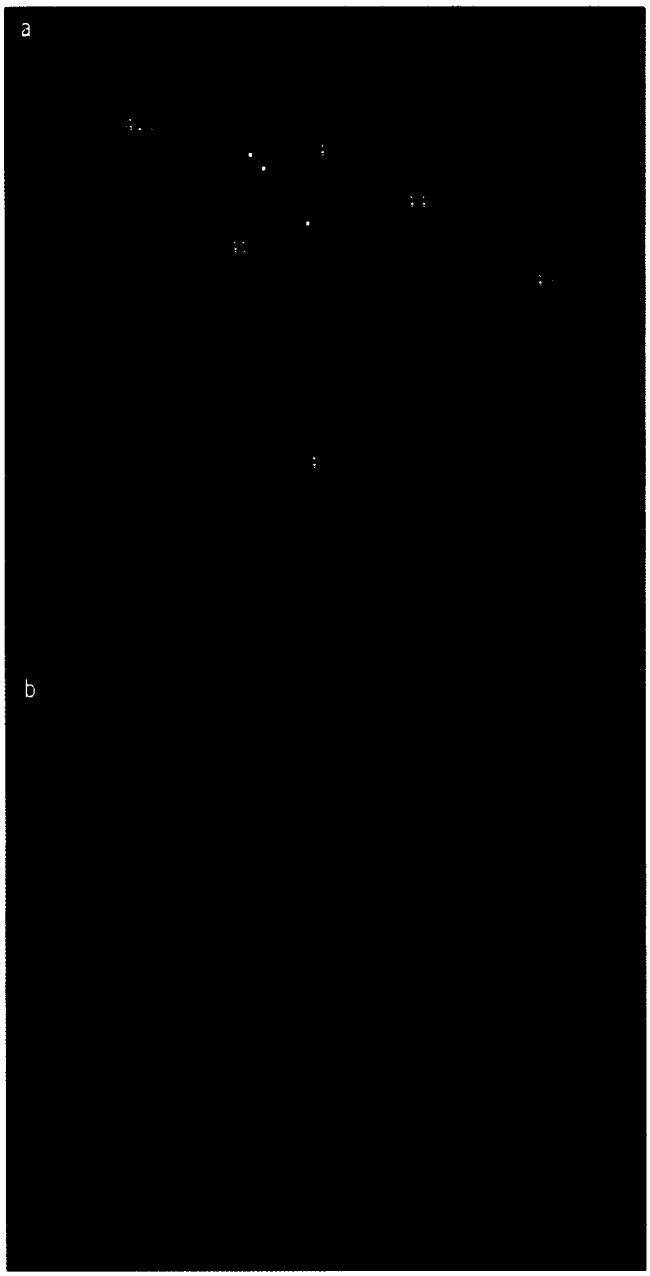

Figure 6. The secondary structure of the five-way junction (5WJ) is represented (a) with an arrangement as close as possible to the 3-D structure model and (b) to stress the role of the crosslink 31–48 in helping the choice of stems for stacking. The red and orange junctions are crossed only in the secondary structure diagram. The internal loop of H16 was modelled with two consecutive AA-platform (white frame)[49] and three non-canonical base-pairs (open squares) flanked with two G·U pairs (filled squares).

strands of H18 and the junction between the 5′-strand of $Pk2_2$ and the 3′-strand of $Pk2_1$ are, respectively, shielded by ribosomal protein S4 and S12. H16 and H17, for which canonical base-pairs were preferred to the previously proposed base-triple[42] (Fig. 1), are then coaxially stacked, as suggested by tRNA crystal structures. All residues protected from hydroxyl radical attack by S4 are set on the same side by increasing the angle between the first pair of H16 and H17 from 36° to 45°. This building-block is then placed in a fashion presenting the hit side of H16/H17 to S4. Thus, the best way to add H4 to the model is to stack it on H18 in order to displace it from S4. In a search for the optimal orientation of H4 towards H3 with respect to the crosslink 31–48,[24] free rotation of H4 around the torsional angles of G38 and its flanking residues was envisaged. This study indicated that the feasibility of the crosslink was dependent on a perpendicular orientation of the helices. Such a packing enables C48 to crossover the narrow groove of H3 to meet, at a distance of less than 5 Å, G31 which is located at the opposite side of the hinge (G38) between H3 and H4. In such an orientation, the protections of residues 36–37 due to S12[6] could be rationalized. Furthermore, several non-canonical base-pairs can be formed within the strongly conserved internal loop of H16. These are a 'sheared' G·A pair, G410(N3, N2)·A430(N6, N7), a Hoogsteen *trans* A·U pair, A411(N6, N7)·U429(O2, N3), and a G·G pair, G413(N2; N1)·G428(O6, N7), all likely flanked by two AA-platforms[49] (Fig. 6), while A412 is bulging out. This asymmetrical loop could constitute the motif recognized by S4, as evidenced by the behaviour of H16 towards probing reagents in its presence.[6,50] Recently, a symmetric motif containing non-canonical base pairs including sheared G·As was indicated for the region responsible for the incorporation of selenocysteine in eukaryotic messengers.[51]

The three-way junction

The model of the three-way junction, encompassing helices H4, H5 and H15 (Fig. 7), is based on the use of intra-RNA crosslinks at positions 31/48 and 366–369/397–399 (Table 1). The three helices constitute a Y-shaped structure with H15 stacked on H4 and H5 lying beside H4. The junction 360–366 passes through the shallow groove of H4 as a consequence of the crosslink 366–369/397–399. The pairing of C47 with G361[42] is then very likely but occurs in a context of non-canonical interactions which were investigated by phylogenetic analysis (Table 3). In this context, atoms N2 and N3 of G361 interact with atoms N7 and N6 of A50, respectively. The resulting triple is then sandwiched between two 'sheared' A·G pairs A51·G360 and G362·A366. The latter corresponds to the closure of the loop G(362)AAUA on which H5 stacks, thus without loss of stacking efficiency.

The central junction

The central junction (Fig. 8) is composed of three helices (H3, H19 and H27) and one type (ii) pseudoknot (Pk1). Few RNA–protein crosslinks as well as footprints have been reported and all of the protection patterns depend on the presence of S12 and S16.[5,6] Obviously such patterns cannot be attributed to direct RNA–protein contacts since S16 hits residues spread over the whole 5′ and central domains, while S12 is linked to the 530-loop (Table 1). On the contrary, S5 can be located with confidence in the vicinity of Pk1.[5,52] In order to constrain the modelling of the central

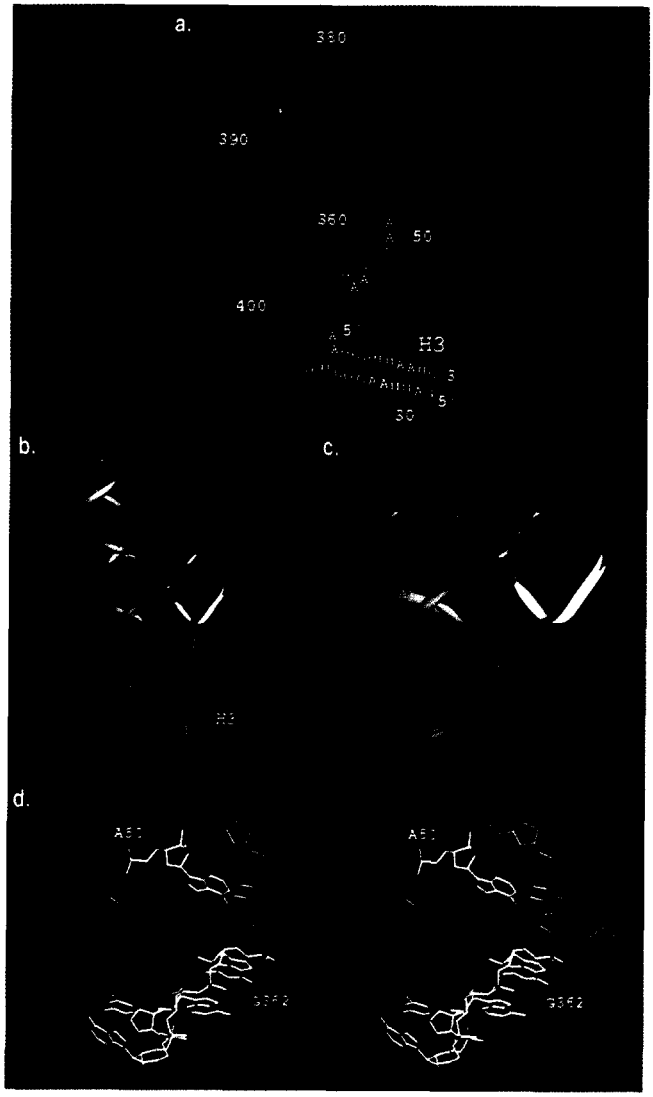

Figure 7. Secondary (a) and ribbon structure (b) of the three-way junction between H4, H5 and H15. The red enlargement (c) illustrates the RNA–RNA crosslinks where bases are drawn as balls and sticks. The bases are A366–A397 (green) and G31–C48 (red) where G31 belongs to H3 (grey). A stereo pair of the motif forming the loop on which H5 stacks is represented in (d). It emphasizes how the base-triple C47–G361·A50 is sandwiched between two sheared A·G pairs (A51·G360 and G362·A366).

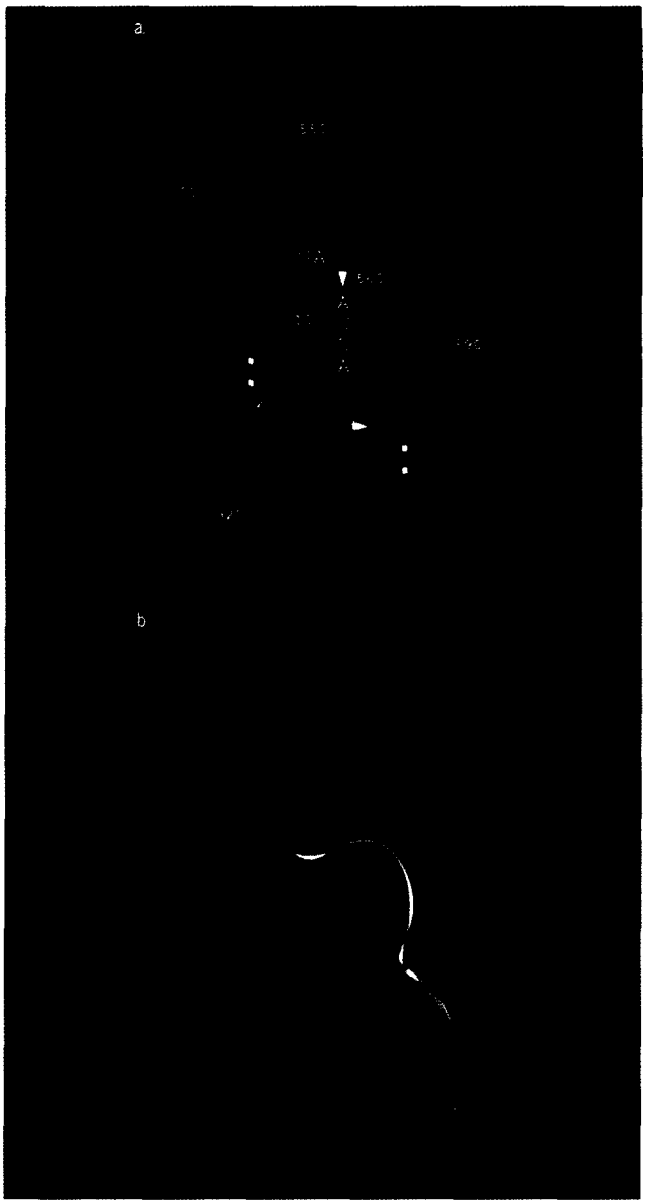

Figure 8. Secondary (a) structure of the central junction where additional base-pairings are indicated. The ribbon structure (b) clearly shows the coaxial stack between helices Pk1 (red) and H3 (purple) as well as between H19 (orange) and H27 (blue). The 557–563 junction (yellow) links H19 through the shallow groove of H27 while the 3′-end of H27 enables the closure of $Pk1_2$. This complex topology leads otherwise to a simple 3-D model.

junction, positions 564–566, 884–886, 888–891, 909–912 in H19 and H27, and the 557–563 junction were subjected to systematic phylogenetic analysis. However, these sequences are strongly conserved, while those which could not base pair in these regions were found to belong to the Bovine (*Bos taurus*) and Nematode (*Ascaris suum, Caenorhabditis elegans*) mitochondria. These symbionts lack the 557–563 junction as well as helices H16 and H17, transforming the five-way junction to a three-way junction. Further analysis showed that the pairing possibilities for bases 564–566/884–886 and 888–891/909–912 were always achieved for 16S rRNAs with a consensus 557–563 junction (Fig. 9). The strong correlation between these events leads us to assume that the absence of the junction 557–563 is correlated with the systematic absence of the basis of stems H19 and H27 (564–566/884–886, and 888–891/909–912). In the model, therefore, residue 556 is within a distance of three to five nucleotides from 567.

The model of Pk1, previously described, is stacked on H3 to avoid the increase of the distance between U920 and S7 (Table 1). H19 is then placed below Pk1 to ease the path of the 3′-domain to the head of the subunit. This position of H19 is suggested by the anchoring of the 840-loop to S18 (Table 1). H27 is then stacked on H19, thus pointing towards the solvent side of the

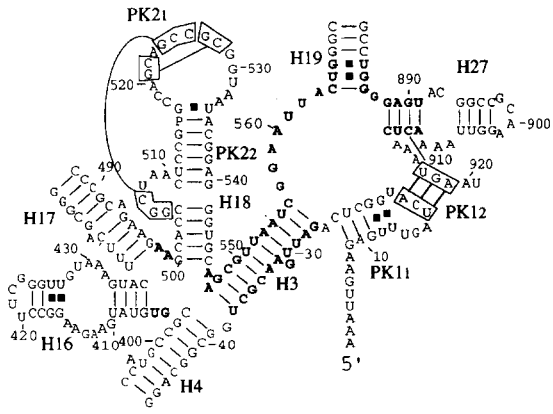

Escherichia coli

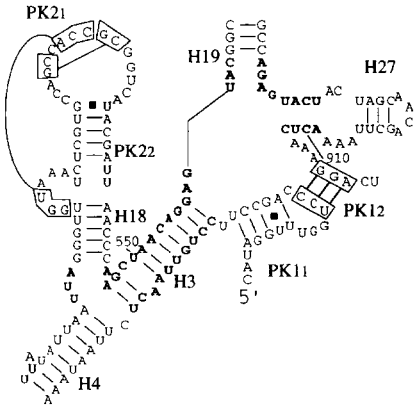

Bos taurus : Mitochondrion

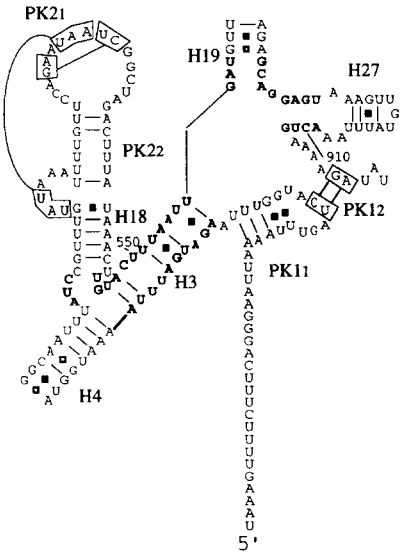

Caenorhabditis elegans (nematode) : Mitochondrion

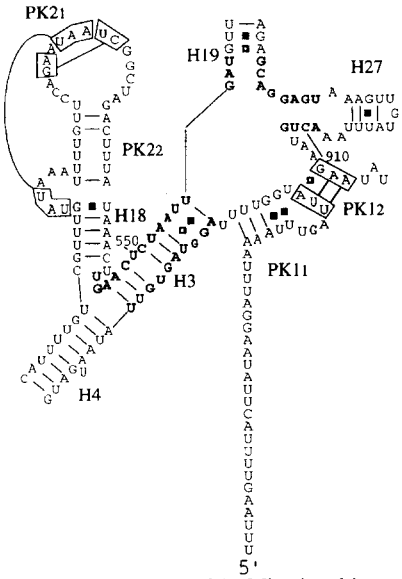

Ascaris suum (nematode) : Mitochondrion

Figure 9. The four different types of secondary structures in the central region. The basis of both H19 and H27 (564–566/884–886) can only be base-paired in a Watson–Crick fashion in the sequence of *E. coli*. In the other sequences, their absence is strongly correlated with the shortening of the 557–563 junction and the deletion of helices H16 and H17.

subunit in a manner that enables its 3′-strand to enclose $Pk1_2$. The resulting central junction is finally shaped as a cruciform-like junction, with the difference that two partners compose the stems of a pseudoknot, changing the topology but not the relative orientation of the helices. This model is supported by different experimental results. Deletion experiments[53] led to the result that H27 is not involved at any translation step, which is consistent with its location at the solvent side of the subunit. Moreover, the curl imposed to the junction 557–563 around Pk1 makes it pass through the shell of S5 in the protein map, a fact consistent with the APAI crosslink between S5 and residues 559–561.[54] In addition, a base-triple is formed between residues A563, G887 and A913, as described in Table 3, providing the stacking continuity between H19 and H27.

Overall description of the model

Pk1 and H3, coaxially stacked along the *x*-axis of the subunit, are forming the neck beside proteins S2 and S5. The building block Pk1/H3 implicates the location of the 5′-domain at the left-side of the body, whereas the central domain is directed towards the platform (right-side). Thus, the 3′-end of the model, which corresponds to the beginning of the 3′-major domain points towards the head, at a distance of about 50 Å from S7 (Table 1). Concerning the 5′-domain, the perpendicular orientation of H3 and H4 enables a

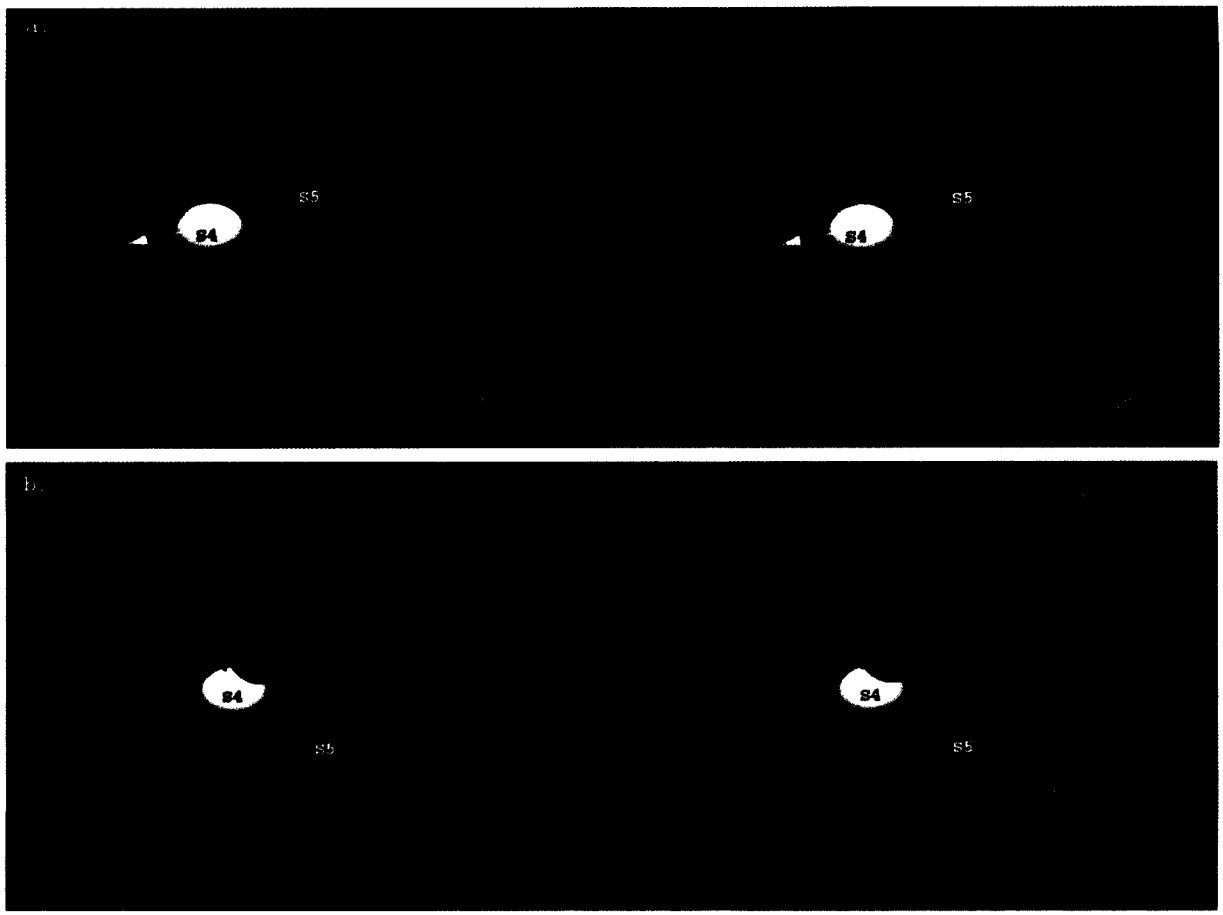

Figure 10. Stereo-pairs of the rRNA core model of the 16S. (a) The crosslink of H16 with S4 is denoted by a yellow arrow, and the agreement with biochemical data is straightforward (see Table 1). The 557–563 junction, which was crosslinked to S5, slightly interpenetrates it. (b) The crosslink of S18 with the 840-loop is denoted with a red arrow (the view was rotated around the x-axis by about 180°). The following colour code was adopted: pseudoknots are red, hairpins are orange. The connecting helices are alternatively blue or purple and the radii of gyration have been reduced by 5 Å for clarity.

coaxial stacking of H4 on H18. As a consequence of the constraints due to the first and second anchor points (Table 1), H4 points backward, locating H5 and H15 on the solvent side. Thus, we assume that the remaining 5′-domain helices (H6–H14) fill the space from the rear-upper part of the body to its bottom, where S17 and S20 are located.[55] The stacking of H18 on H4 puts Pk2 at the subunit interface, while H16/H17 lies at the left side of the subunit in the close vicinity of S4 and S12. Considering the central domain, the short length of the junctions 887 and 913–915 strongly constrains H27 to be stacked on H19. The new building block (H19/H25/H26/Pk3/H27) is then placed below Pk1 along the z-axis (Fig. 10).

Discussion

A 328-residue portion of the 16S rRNA (8–58/354–446/488–571/821–920) which contains three conserved pseudoknots (Fig. 1) has been constructed. The modelling aimed at gaining insight as to how the three pseudoknots fold, are settled into the 30S subunit, and control self-assembly and translation.

Comparisons with other models

Even though our model does not take into account the whole 16S molecule, it is interesting to compare it to the previously published ones[5,17,18] since it contains topological novelties implying a different distribution of the 16S-core within the 30S subunit.

Pk1 occupies the geometrical centre of the subunit and is stacked on H3 along the x-axis. As observed in the other models, the loop 14–20 is oriented towards S7 while G38 is located near S4, locating the building block Pk1/H3 in the neck. The relative placement of H4 and H3 constitutes the first topological difference with the other models where H4 is parallel to H3 and located from S4 to the 50S interface. Instead, we considered that the location of H4 depends on the crosslink 31–48, which partially constrains the conformation of the 5-way junction (5WJ). This results in the stacking of H4 on H18, whereas H18/Pk2 is oriented from S4 to S12 at the 50S interface. Our arrangement therefore orients H4 backward from S4 and to the location of H5 and H15 in the left part of the 30S body on the solvent side. Thus, according to footprint experiments,[6] the missing helices (H6–H14) are clustered within the region encompassed

by H5 and the bottom of the 30S particle (S17 and S20). Moreover, this low-resolution localization of the 5′-domain provides a good explanation for the density of mass in that region of the subunit.[56,57] The removal of the major part of the 5′-domain from the intersubunit space in our model is supported by the fact that no crosslink could be observed between the 5′-domain and the mRNA or the tRNA.[23]

The other major topological difference consists in the location of H27 which points to the solvent side rather than in the region surrounded by proteins from the 50S subunit interface (S12, S16, S18 and S21) as in previous models. This hairpin was placed on the basis of biological results showing the independence of in vitro translation rate on the partial or complete deletion of H27.[53] Base-probe footprint experiments[5] yield many indirect protein-mediated protections, as supported by the results of Powers[6] which show no FeII–EDTA footprint on H27. Moreover, comparative sequence analysis of the central junction indicated that the terminal bases of helices H19 (564–566/884–886) and H27 (888–891/909–912) were likely to pair in a molecule with a consensus 557–563 junction. The closures of H19 and H27, together with the constraints due to the crosslink of S5 with A559[54] and with the length of the junction 913–915, compel H27 to stack on H19 and to point to the solvent instead of towards the 50S interface as in previous models. Our conclusion is supported by the following experiments. The first one[58] reports the crosslink of ribosomal protein S1 to the region 861–889 which is located, in our model, in the sphere occupied by S1 at the rear-side of the subunit.[15,16] The second result[59] consists of the crosslink between H27 and the 300-region of the 5′-domain, which should both lie, as concluded from our modelling studies, at the rear-side of the subunit.

Roles of pseudoknots in the control of self-assembly and translation

The model illustrates the cluster organization of the three pseudoknots in the 30S particle. Remarkably, two of them (Pk1 and Pk3) are buried in the subunit while the remaining (Pk2) lies at the 50S interface, accessible to the solvent. Two states were built for the 530-loop, without and with a pseudoknot (Pk2). This is in agreement with data from chemical probing[5,19] and phylogenetic conservations,[42] as well as with functional observations (reviewed in the literature[30]) that lead to an intricate net of contacts between the 530-loop, ribosomal protein S12, and elongation factor Tu. The role of the pseudoknot of the central domain (Pk3) seems also to be most important for ribosomal dynamics. Although Pk3 is formed between residues fairly remote in sequence, its closure constrains only the positioning of helices H19, H25, H26 and Pk3. The connection of H26 with S18, located at the subunit interface, leads to the suggestion that the change from a tight to a loose conformation could trigger a pivotal mechanism at some translation step. Recently, large conformational changes between the isolated and bound 30S particles were observed and related to processes occurring between the initiation and translation complexes.[60] The modelling of the central junction suggests strongly that Pk1 is structurally crucial in particle self-assembly besides its role in initiation of translation.[10] The experimental footprints obtained by Powers et al.[4] indicate that the folding of Pk1 and of the central junction occur at the later stages of 16S rRNA folding. This folding scheme might be completed by the observation that the *E. coli* ribosomal RNA leader *nut* region binds to the 16S rRNA 5′-end.[61] In vivo, such an RNA–RNA binding might prevent trapping of the 16S rRNA in alternative folding forms and thus could play the role of a delay mechanism in the overall self-assembly.

Experimental

The molecular modelling method is as described in ref 62. The *E. coli* 16S secondary structures are from the Ribosomal Database Project (RDP)[37] with slight changes in the tertiary interactions discussed in text. All covariations and statistical analyses of sequences were made with the program COSEQ written by C. Massire. The independent atomic 2-D structure elements were built with the programs FRAGMENT, NAHELIX and PSEUDOKNOT. The 3-D generated elements were then linked together, incorporating the biochemical data, interactively using the software FRODO[63,64] designed for nucleic acid modelling (STG version),[65] which is running on a PS300 Evans and Sutherland graphical system hooked to a Vax750. The resulting working models were then subjected to stereochemical and geometrical refinement in order to insure proper geometry and to prevent bad contacts using the Konnert–Hendrickson[66] restrained least-squares refinement program NUCLIN/NUCLSQ.[67] Color pictures were designed with the software DRAWNA.[68] The coordinates (16S_core.brk) are available by anonymous ftp (130.79.17.244) in directory (cd/pub).

Acknowledgements

We thank Christian Massire for help with the program COSEQ that he developed for analysis of covariations in aligned sequences and Luc Jaeger for critical reading of the manuscript. B.M. is supported by a Bourse Docteur Ingénieur Rhône–Poulenc Rorer and CNRS.

References

1. Nomura, M.; Held, W. A. *Ribosomes*; Nomura, M.; Tissieres, A.; Lengyel, P., Eds.; Cold Spring Harbor Laboratory: New York, 1974; pp 193–223.

2. Held, W. A.; Ballou, B.; Mizushima, A.; Nomura, M. *J. Biol. Chem.* **1974**, *249*, 3103.

3. Mizushima, S.; Nomura, M. *Nature (London)* **1970**, *226*, 1214.

4. Powers, T.; Daubresse, G.; Noller, H. F. *J. Mol. Biol.* **1993**, *232*, 362.

5. Stern, S.; Weiser, B.; Noller, H. F. *J. Mol. Biol.* **1988**, *204*, 447.

6. Powers, T.; Noller, H. F. *RNA* **1995**, *1*, 194.

7. Woese, C. R.; Gutell, R. R.; Gupta, R.; Noller, H. F. *Microbiol. Rev.* **1983**, *47*, 621.

8. Woese, C. R.; Gutell, R. R. *Proc. Natl. Acad. Sci. U.S.A.* **1989**, *86*, 3119.

9. Gutell, R. R.; Noller, H. F.; Woese, C. R. *EMBO J.* **1986**, *5*, 1111.

10. Brink, M. F.; Verbeet, M. P.; de Boer, H. *EMBO J.* **1993**, *12*, 3987.

11. Powers, T.; Noller, H. F. *EMBO J.* **1991**, *10*, 2203.

12. Vila, A.; Viril-Farley, J.; Tapprich, W. E. *Biochem.* **1994**, *91*, 11148.

13. Westhof, E.; Jaeger, L. *Curr. Op. Struct. Biol.* **1992**, *2*, 32.

14. Westhof, E.; Masquida, B.; Jaeger, L. *Folding & Design* **1996**, *1*, R78.

15. Capel, M. S.; Engelman, D. M.; Freeborn, B. R. *Science* **1987**, *238*, 1403.

16. Capel, M. S.; Kjeldgaard, M.; Engelman, D. M.; Moore, P. B. *J. Mol. Biol.* **1988**, *200*, 65.

17. Brimacombe, R.; Atmadja, J.; Stiege, W.; Schüler, D. *J. Mol. Biol.* **1988**, *199*, 115.

18. Malhotra, A.; Harvey, S. C. *J. Mol. Biol.* **1994**, *240*, 308.

19. Powers, T.; Stern, S.; Changchien, L. M.; Noller, H. F. *J Mol Biol* **1988**, *201*, 697.

20. Powers, T.; Craven, G. R.; Changchien, L. M.; Noller, H. F. *J. Mol. Biol.* **1988**, *200*, 309.

21. Stern, S.; Changchien, L. M.; Craven, G. R.; Noller, H. F. *J. Mol. Biol.* **1988**, *200*, 291.

22. Stern, S.; Powers, T.; Changchien, L. M.; Noller, H. F. *J. Mol. Biol.* **1988**, *201*, 683.

23. Brimacombe, R. *Eur. J. Biochem.* **1995**, *230*, 365.

24. Stiege, W.; Atmadja, J.; Zobawa, M.; Brimacombe, R. *J. Mol. Biol.* **1986**, *191*, 135.

25. Gauthier, A.; Turmel, M.; Lemieux, C. *Mol. Gen. Genet.* **1988**, *214*, 192.

26. Fromm, H.; Galun, E.; Edelmann, M. *Plant Mol. Biol.* **1989**, *12*, 499.

27. Bryan, L. E.; van den Elzen, H. M. *Antimicrob. Ag. Chem.* **1977**, *12*, 163.

28. Allen, P. N.; Noller, H. F. *J. Mol. Biol.* **1989**, *208*, 457.

29. Bonny, C.; Montandon, P. E.; Marc, M. S.; Stutz, E. *Biochem. Biophys. Acta* **1991**, *1089*, 213.

30. Powers, T.; Noller, H. F. *TIG* **1994**, *10*, 27.

31. Oakes, M. I.; Lake, J. A. *J. Mol. Biol.* **1990**, *211*, 897.

32. Winklemann, D. A.; Kahan, L.; Lake, J. A. *Proc. Natl. Acad. Sci. U.S.A.* **1982**, *79*, 5184.

33. Atmadja, J.; Brimacombe, R.; Blöcker, R.; Franck, R. *Nuc. Ac. Res.* **1985**, *13*, 6919.

34. Ramakrishnan, V.; White, S. W. *Nature (London)* **1992**, *358*, 768.

35. Lindahl, M.; Svensson, L. A.; Liljas, A.; Sedelnikova, S. E.; Eliseikina, I. A.; Fomenkova, N. P.; Nikonov, S. V.; Garber, M. B.; Muranova, T. A. *EMBO J.* **1994**, *13*, 1249.

36. Jaishree, T. N.; Ramakrishnan, V.; White, S. W. *Biochem.* **1996**, *35*, 2845.

37. Maidak, B. L.; Olsen, G. J.; Larsen, N.; Overbeek, R.; McCaughey, M. J.; Woese, C. R. *Nuc. Ac. Res.* **1996**, *24*, 82.

38. Pley, H. W.; Flaherty, K. M.; McKay, D. B. *Nature (London)* **1994**, *372*, 68.

39. Scott, W. G.; Finch, J. T.; Klug, A. *Cell* **1995**, *81*, 991.

40. Ueda, T.; Suzuki, T.; Yokogawa, K.; Watanabe, K. *Biochimie* **1994**, *76*, 1217.

41. Moazed, D.; Stern, S.; Noller, H. F. *J. Mol. Biol.* **1986**, *187*, 399.

42. Gutell, R. R.; Larsen, N.; Woese, C. R. *Microbiol. Rev.* **1994**, *58*, 10.

43. Van Ryk, D. I.; Dahlberg, A. E. *Nucl. Acid Res.* **1995**, *23*, 3563.

44. Powers, T.; Noller, H. F. *Proc. Natl. Acad. Sci. U.S.A.* **1993**, *90*, 1364.

45. Chou, S.-H.; Cheng, J.-W.; Reid, B. R. *J. Mol. Biol.* **1992**, *228*, 138.

46. Taylor, R.; Kennard, O. *J. Am. Chem. Soc.* **1982**, *104*, 5063.

47. Michel, F.; Costa, M. *RNA Structure and Function*; Simons, R. W.; Grunberg-Manago, M., Eds.; Cold Spring Harbor Laboratory: New York, 1996; in press.

48. Cate, J. H.; Gooding, A. R.; Podell, E.; Zhou, K.; Golden, B. L.; Kundrot, C. E.; Cech, T. R.; Doudna, J. A. *Science* **1996**, *273*, 1678.

49. Cate, J. H.; Gooding, A. R.; Podell, E.; Zhou, K.; Golden, B. L.; Szewczak, A. A.; Kundrot, C. E.; Cech, T. R.; Doudna, J. A. *Science* **1996**, *273*, 1696.

50. Heilek, G. M.; Marusak, R.; Meares, C. F.; Noller, H. F. *Proc. Natl. Acad. Sci. U.S.A.* **1995**, *92*, 1113.

51. Walczak, R.; Westhof, E.; Carbon, P.; Krol, A. *RNA* **1996**, *2*, 354.

52. Heilek, G.; Noller, H. *Science* **1996**, *272*, 1659.

53. Gravel, M.; Leclerc, D.; Melancon, P.; Brakier, G. L. *Nucl. Acid Res.* **1989**, *17*, 2723.

54. Osswald, M.; Greuer, B.; Brimacombe, R.; Stöffler, G.; Bäumert, H.; Fasold, H. *Nucl. Acid Res.* **1987**, *15*, 3221.

55. Schwedler, G.; Albrecht, E. R.; Rak, K. H. *Eur. J. Biochem.* **1993**, *217*, 361.

56. Stark, H.; Mueller, F.; Orlova, E. V.; Schatz, M.; Dube, P.; Erdemir, T.; Zemlin, F.; Brimacombe, R.; Van Heel, M. *Structure* **1995**, *3*, 815.

57. Franck, J.; Zhu, J.; Penczek, P.; Li, Y.; Srivastava, S.; Verschoor, A.; Radermacher, M.; Grassucci, R.; Lata, R. K.; Agrawal, R. K. *Nature (London)* **1995**, *376*, 441.

58. Golinska, B.; Millon, R.; Backendorf, C.; Ebel, J. P.; Ehresmann, B. *Eur. J. Biochem.* **1981**, *115*, 479.

59. Brimacombe, R.; Greuer, B.; Mitchell, P.; Osswald, M.; Rinke-Appel, J.; Schüler, D.; Stade, K. *The Ribosome, Structure, Function, and Evolution*; Hill, W. E.; Moore, P. B.; Dahlberg, A.; Schlessinger, D.; Garrett, R. A.; Warner, J. R., Eds.; American Society for Microbiology: Washington DC, 1990; pp 93–106.

60. Lata, K. R.; Agrawal, R. K.; Penczek, P.; Grassucci, R.; Zhu, J.; Franck, J. *J. Mol. Biol.* **1996**, *262*, 43.

61. Pardon, B.; Wagner, R. *Nucl. Acid Res.* **1995**, *23*, 932.

62. Westhof, E. *J. Mol. Struct.* **1993**, *286*, 203.

63. Jones, T. A. *J. Appl. Cryst.* **1978**, *11*, 268.

64. Pflugrath, J. W.; Saper, M. A.; Quiocho, F. A. *J. Mol. Graphics* **1983**, *1*, 53.

65. Amerein, B.; Ripp, R.; Dumas, P. *J. Mol. Graphics* **1987**, *5*, 184.

66. Konnert, J. H.; Hendrickson, W. A. *Acta Cryst.* **1980**, *A36*, 344.

67. Westhof, E.; Dumas, P.; Moras, D. *J. Mol. Biol.* **1985**, *184*, 119.

68. Massire, C.; Gaspin, C.; Westhof, E. *J. Mol. Graphics* **1994**, *12*, 201.

69. Powers, T.; Noller, H. F. *J. Mol. Biol.* **1994**, *235*, 156.

70. Greuer, B.; Osswald, M.; Brimacombe, R.; Stöffler, G. *Nucl. Acid Res.* **1987**, *15*, 3241.

71. Stöffler–Meilicke, M.; Stöffler, G. *The Ribosome, Structure, Function, and Evolution*; Hill, W. E.; Moore, P. B.; Dahlberg, A.; Schlessinger, D.; Garrett, R. A.; Warner, J. R., Eds.; American Society for Microbiology: Washington, DC, 1990; pp 123–133.

72. Oakes, M. I.; Kahan, L.; Lake, J. A. *J. Mol. Biol.* **1990**, *211*, 907.

73. Wower, I.; Brimacombe, R. *Nuc. Ac. Res.* **1983**, *11*, 1419.

(*Received in U.S.A.* 26 *September* 1996; *accepted* 18 *February* 1997)